Characterization of the OPAL Obscurant Penetrating LiDAR in various Degraded Visual Environments

Evan Trickey[*], Philip Church[**], Xiaoying Cao[***]
Neptec Design Group, 302 Legget Drive, Kanata, Ontario, Canada K2K 1Y5

ABSTRACT

The OPAL obscurant penetrating LiDAR was developed by Neptec and characterized in various degraded visual environments (DVE) over the past five years. Quantitative evaluations of obscurant penetration were performed using the Defence R&D Canada – Valcartier (DRDC Valcartier) instrumented aerosol chamber for obscurants such as dust and fog. Experiments were done with the sensor both at a standoff distance and totally engulfed in the obscurants. Field trials were also done to characterize the sensor in snow conditions and in smoke. Finally, the OPAL was also mounted on a Bell 412 helicopter to characterize its dust penetration capabilities, in environment such as Yuma Proving Ground. The paper provides a summary of the results of the OPAL evaluations demonstrating it to be a true "see through" obscurant penetrating LiDAR and explores commercial applications of the technology.

Keywords: DVE, LiDAR, Obscurants Penetration, Panoramic LiDAR.

1. INTRODUCTION

Helicopter pilots can encounter situations of Degraded Visual Environments (DVE) when they land or take-off in the presence of obscurants such as dust, snow, fog and smoke. Under these conditions, pilots cannot see nearby objects that provide the visual references necessary to control the aircraft near the ground. There are many reported rotary wing accidents and maintenance costs due to brownout[1].

Several sensing technologies have been evaluated to improve pilot situational awareness in DVE[2]. Millimeter-wave radar (MMW) can penetrate obscurants well due to their long wavelength but are limited in their spatial resolution capability. LiDAR have shorter penetration depths when compared to MMW radars, but can offer higher spatial resolution sufficient to detect small threats to the aircraft, such as wires, terrain depressions in the landing zone and small size objects lying in the landing zone[3,4,5]. Other optical technologies, such as infrared cameras and Flash Ladar[6] have also been evaluated for that purpose.

The OPAL LiDAR developed by NEPTEC is specifically designed for aerosol penetration with its unique optics and electronics, and has been subjected to several field evaluations for a variety of obscurants. The paper will present the underlying obscurant penetrating technology, along with experimental results and theoretical prediction data. Sensor advances currently in development will also be discussed as well as its commercial applications.

2. OBSCURANTS PENETRATION

This section presents the OPAL technology background.

2.1 OPAL LiDAR Technology Background

The OPAL LiDAR has been developed in view of providing a true see-through capability for pilots in the final approach of a landing zone (LZ). The technical approach rests on these important elements: a high power pulsed laser emitter combined with a sensitive receiver, an optical design that rejects the backscattered light from nearby obscurant particles, a capability to extract target signals engulfed in a cloud of obscurants and an efficient filtering of noise caused by the reflection of light on obscurants.

[*] etrickey@neptec.com ; phone (613) 599-7603 (x487); fax (613) 599-7604
[**] pchurch@neptec.com; phone (613) 599-7603 (x513); fax (613) 599-7604
[***] xiaoyingcao33@gmail.com phone: (613) 599-7603 (x494)

High power pulsed laser with peak power of the order of 10kW are commercially available while APD receivers can provide detection limit of the order of few tens of nW. The ratio of the launch power to the return power on the receiver can be as high as 10^{12} while the dynamic range of the receiver electronics is normally less than 10^{5} (50dB). This illustrates the importance of using an optical design that will suppress the backscatter from nearby aerosol. The OPAL LiDAR optical design suppresses signals originating from the first three meters in front of the sensor aperture.

Figure 1 below illustrates a full waveform return in the presence of obscurants. The signal will typically show a sharp rise from the reflection of nearby obscurants and slowly decrease over the distance. Targets engulfed in the obscurant cloud may or may not appear later in the signal, depending on the reflectivity of the target and the density of the obscurants. The processing of the full waveform return in view of extracting the signal is ideal. However, this entails the acquisition and processing of a large amount of data. In order to be useful for helicopter situational awareness, this needs to be achieved in real-time with very little latency. This amount of real-time processing becomes challenging and costly. Other methods have been developed for the OPAL LIDAR in order to extract in real-time target signals in the waveform without resorting to a full digitization of the waveform[5].

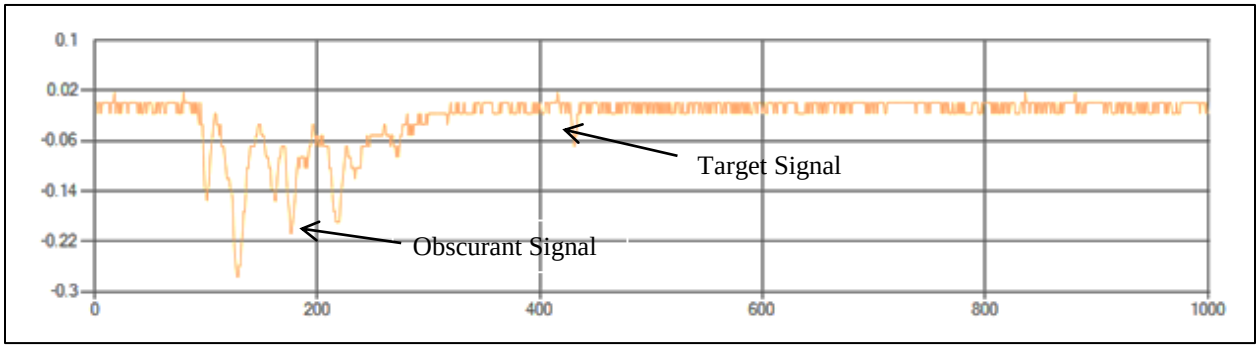

Figure 1. Example of a full LiDAR waveform return in obscurant

The quantity of light scattered by an obscurant particle is proportional to the area of the particle and is given by the following relation:

$$A = Q\pi r^2 \qquad (1)$$

Where,

A: The effective scattering area
Q: The scattering efficiency
r: The radius of the particle.

Figure 2 shows how the scattering efficiency Q varies as a function of a size parameter, X, expressed as the ratio of the particle diameter to the wavelength used by the sensor. As an example, for typical fine dust particles of 20μm size, Q would be of the order of 2 for a LiDAR operating at a wavelength of 1.54μm. As a comparison, a millimeter wave (MMW) Radar operating with a wavelength of 94GHz in the same conditions would have a scattering efficiency of about $1.5x10^{-8}$, essentially not being affected by the dust. Therefore, significant obscurant scattering will be present as noise in the LiDAR 3D imagery and it is important to filter out that noise.

Neptec has developed a spatial-temporal filter that uses the properties of obscurant particles to remove more than 99% of the data associated with dust.

Figure 3 shows an example of the filter capabilities, with 3D LiDAR data acquired from a Bell 412 helicopter hovering over dusty ground in Yuma Proving Ground. For ease of representation, the ground data are colored in gray, the obstacles above ground are in red and the data corresponding to returns from dust particles are shown in yellow. The picture below shows the data after the application of the filter, leaving the obstacles and removing the dust data. The filter runs in real-time.

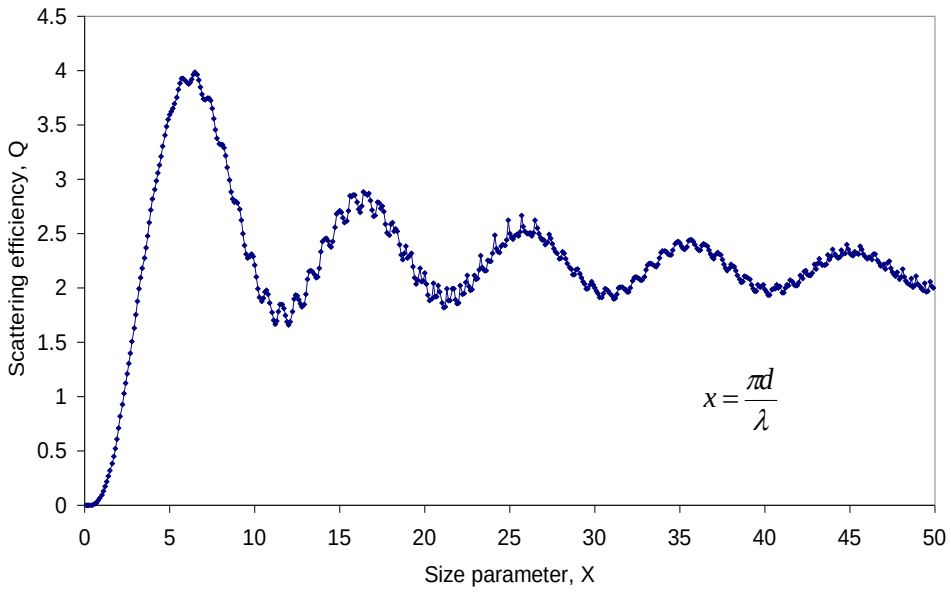

Figure 2. Scattering efficiency versus the size parameter

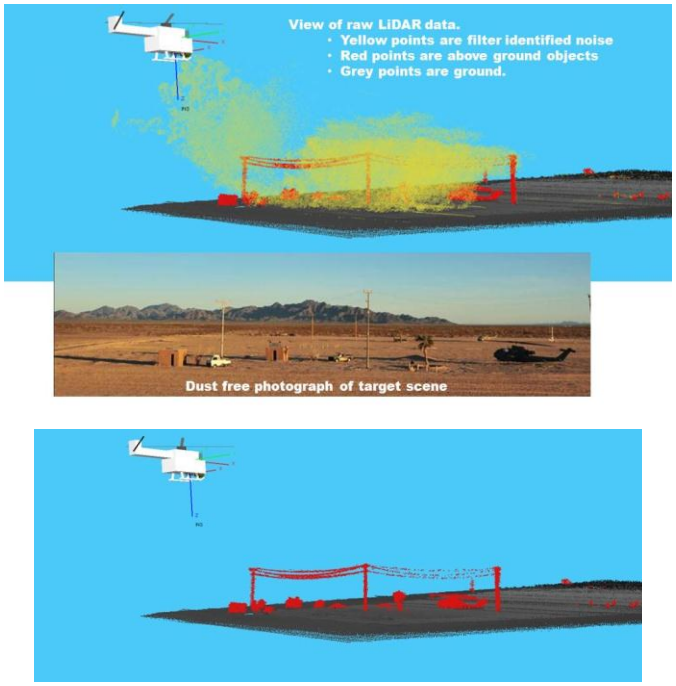

Figure 3. Example of real-time obscurant filtering. Top picture shows in red targets above the ground, in gray the ground and in yellow the noise caused by reflection of the laser light on obscurants. The right bottom picture shows the same scene after application of the filter.

3. OBSCURANT PENETRATION PERFORMANCES

3.1 Predictive Model for Aerosols

In dense aerosols, the laser light pulse goes through multiple scattering events that are better modeled by Monte Carlo simulations. As a first approximation, the LiDAR equation for a single scattering process is used[7]. This is given by:

$$P(R) = P_0 \times \frac{c\tau}{2} \times \beta(R) \times K(R) \times \frac{A}{R^2} \times \exp[-2\int_0^R \alpha(R')dR'] \quad (2)$$

Where $P(R)$ is the LIDAR return from scattering at range R, P_0 is the LIDAR launch pulse power, c is the light velocity, τ is the LIDAR pulse width, $\beta(R)$ is the back scattering coefficient, $\alpha(R)$ is the extinction coefficient, $K(R)$ is the overlap function, A is the receiving lens area and R is the range.

For a uniform aerosol cloud, $\beta(R)$ and $\alpha(R)$ are constants and independent of range. $P(R)$ is shown to be proportional to $exp(-2\alpha R)/ R^2$ and it decreases very fast when range R increases. The equation shows that even for a moderate $\alpha = 0.05/m$, $P(R)$ decreases more than 8 orders of magnitude from 1m range to 100m range, while the return signal decreases only 4 orders of magnitudes at 100m without aerosol attenuation.

3.3 Controlled Performance Evaluations

A series of evaluations were conducted using the aerosol chamber facility at DRDC Valcartier in Quebec, Canada. The corridor has a length of 22m. The optical depth (defined as $-ln(T)$, T is the transmittance) of the aerosol clouds generated by the corridor ranges from 0.01 to over 10, but the range that can be monitored by a transmissometer is 0.01 to 4. The aerosol chamber was used to evaluate laser propagation in MIL-810 dust and water fog.

Figure 4 shows a picture of the aerosol chamber filled with various targets at known distances and the resulting LiDAR data obtained through the dust. The bright light appearing in the bottom picture corresponds to the transmissometer.

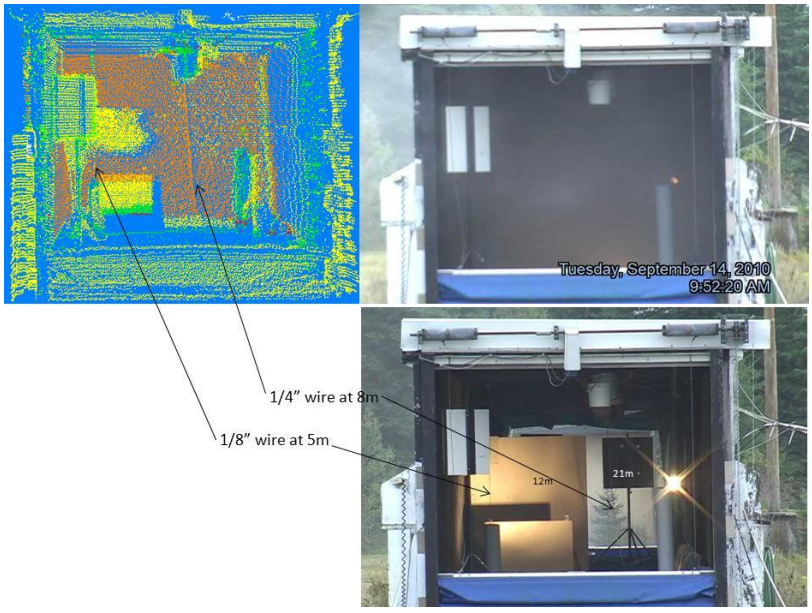

Figure 4. Picture of the aerosol chamber at DRDC Valcartier. Bottom picture shows the opening of the chamber with various targets installed at different ranges. The top left picture shows the chamber filled with dust while the left image corresponds to the OPAL LiDAR data showing various targets, including a ¼" wire at 8m and a 1/8" wire at 5m.

3.3.1 *Dust Penetration Performance*

Dust penetration evaluations with the aerosol chamber were done mostly with the MIL-810 dust which has characteristics similar to several desertic theaters of operation. Arizona road dust type was also used, with similar penetration performances. Figure 5 shows penetration performances obtained for the MIL-810 dust type. The left graph shows a couple of experimental results obtained for dust concentration of 2.3g/m^3 and 3.1g/m^3 respectively. This is compared to theoretical penetration prediction using the LiDAR equation (2). The graph shows two penetration prediction curves based on 20μm and 10μm particle sizes, at a standoff distance of 43m from the dust. The mass extinction coefficients used in equation (2) are determined from the Mie light scattering model, using a given particle size and the wavelength of 1540nm used by the OPAL LIDAR.

The MIL-810 dust has an average particle size which is close to 20μm. The graph shows that the experimental data fall in between those two penetration prediction curves. The right graph compares the penetration prediction for particles size of 20μm with the expected naked eye visibility assuming a transmittance of 0.05. The predictions are calculated for the condition of full immersion into the dust (i.e. 0m standoff distance). In this particular case, the LiDAR penetration will offer most benefits through heavy obscurants at short distances, showing penetration ranges of 2-3 times the naked eye visibility range at distances within few tens of meters. In this example, the LiDAR penetration capability equates the naked visibility at a range of about 200m.

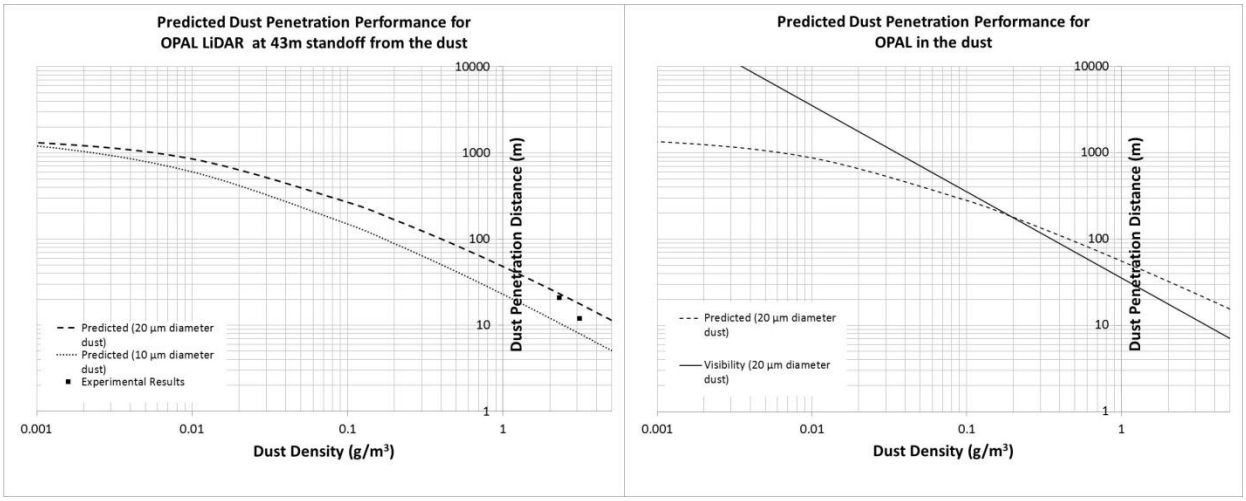

Figure 5. Left graph shows experimental data obtained for the MIL-810 dust compared to predicted penetration using 20μm and 10μm dust particle sizes respectively. Right graph compares naked eye visibility with predicted penetration for a 20μm dust particle size.

3.3.2 Fog Penetration Performance

The aerosol chamber is also capable to generate water fog using high pressure nozzles distributed over the chamber. The left graph in Figure 6 shows experimental results obtained for very dense water fogs. This is compared to theoretical penetration prediction using the LiDAR equation (2), for 10μm fog particle sizes at a standoff distance of 46m from the fog. The exact size distribution of the water fog generated for the experiments is unknown; however a 10μm average fog particle size appears to fit the data well. The right graph compares the penetration prediction for fog particles size of 10μm with the expected naked eye visibility assuming a transmittance of 0.05. The predictions are calculated for the condition of full immersion into the fog (i.e. 0m standoff distance). Similarly to the dust case, the LiDAR penetration will offer most benefits through heavy fog at short distances, showing penetration ranges of about 2 times the naked eye visibility range at short distances. In this example, the LiDAR penetration capability equates the naked visibility at a range of about 90m.

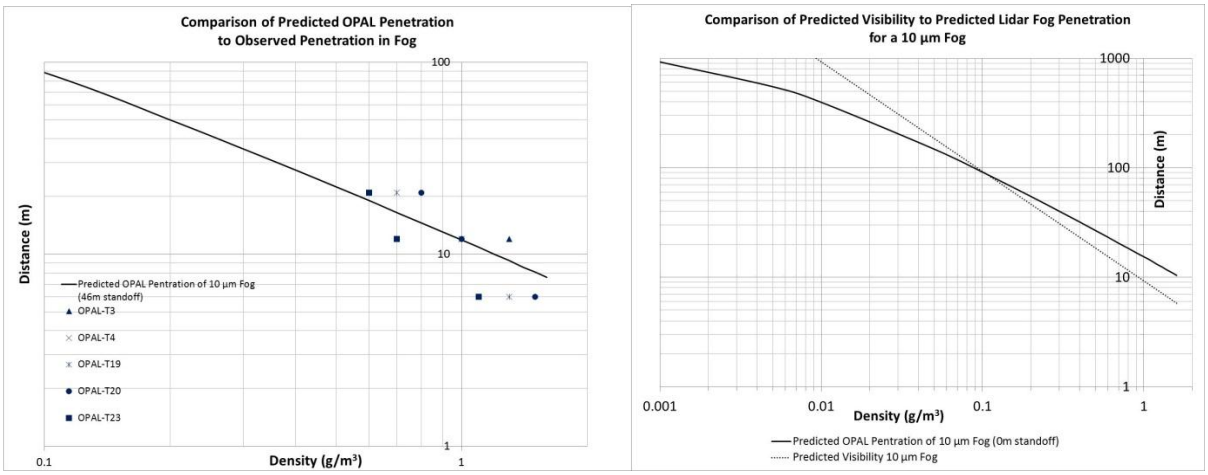

Figure 6. Left graph shows experimental data obtained for very dense water fog compared to predicted penetration using 10µm fog particle size. Right graph compares naked eye visibility with predicted penetration for a 10µm fog particle size.

3.3.3 Whiteout Penetration Performance

Evaluation tests have been carried out with DRDC Valcartier[2] to evaluate the capabilities of the OPAL LiDAR to penetrate heavy snow whiteouts. Figure 7 shows an example of the results obtained using white and black targets installed in a snow field. A heavy snow whiteout was created using a low flying helicopter over a snow covered field and immersing the sensor and targets. The picture at the bottom right shows the OPAL point cloud. Targets located at 56m and 66m inside the whiteout were detected by the system. Due to the nature of those experiments, the whiteout density was not quantified.

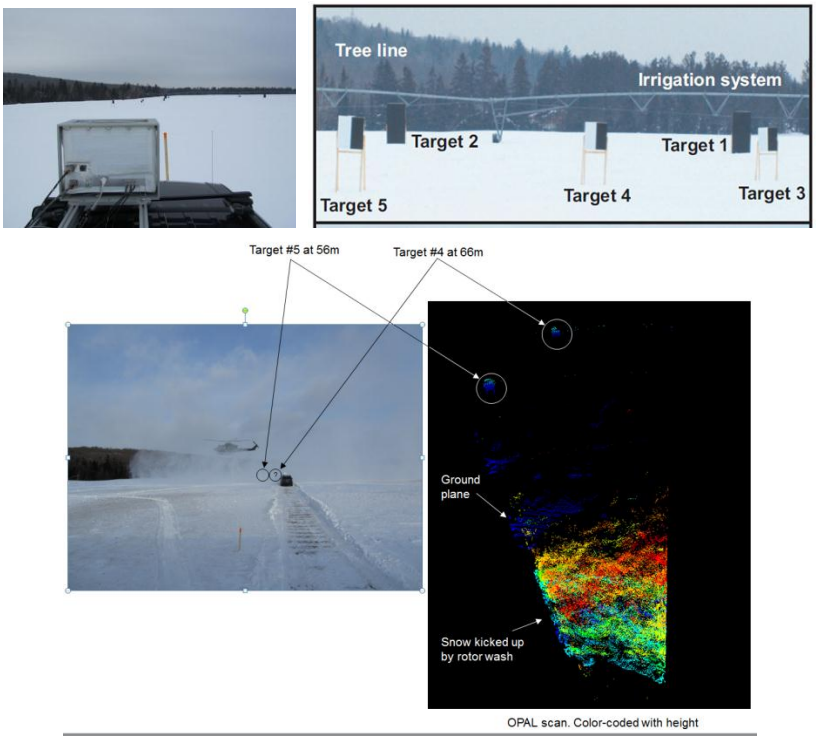

Figure 7. OPAL LiDAR tests in a snow whiteout created by a low flying helicopter[2]. Targets at 56 and 66m from the sensor were detected.

3.3.4 Smoke Penetration Performance

Figure 8 shows an example of tests carried out in smoke for the Department of Defense (DOD). The smoke was generated in a tent at a 1000 feet standoff distance from the sensor. The bottom left picture shows the targets installed in the tent while the upper left picture shows the resulting zero visibility conditions with the smoke. The picture on the right illustrates the sensor point cloud data, colour-coded by range from the sensor. Objects correspondence with the picture is shown with arrows. Due to the nature of those experiments, the smoke density was not quantified. The smoke containment depth was limited to 20 feet due to the size of the tent.

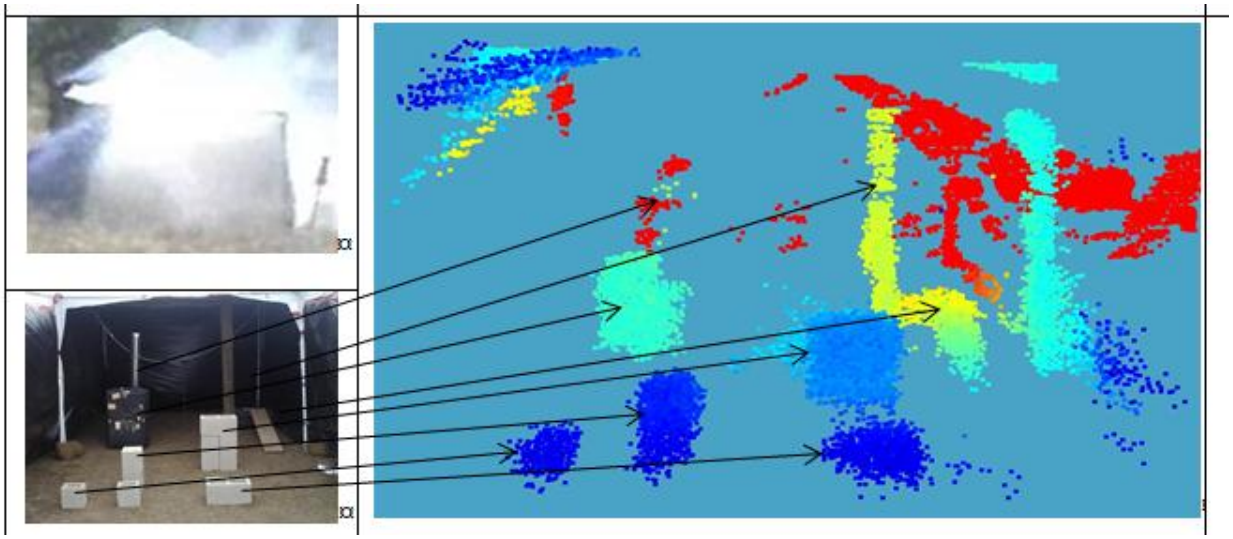

Figure 8. Results obtained in zero-visibility smoke conditions

3.4 Penetration Performance Summary

Figure 9 illustrates few examples of obscurants measured penetration ranges compared with the predicted penetration ranges using equation (2). The mass extinction coefficients were derived from the Mie scattering model for a laser wavelength of 1540nm and using particles properties, such as their expected size.

For the case of dense dust, a particle size of 20μm is used for the model, with the sensor at a standoff distance of 43m from the dust cloud. Experiments were conducted with the MIL-810 dust that has an average particle size of 20μm. The agreement between the model and the measurements is good; however, in reality there is a particle size distribution that will affect the penetration characteristics and this is not accounted for by the current model. In addition, the model assumes an obscurant cloud with a constant density, which is not always the case in reality.

For the case of dense water fog, a particle size of 10μm is used for the model, with the sensor at a standoff distance of 46m. The agreement between the model and the measurements is good; however, in reality the water fog also has a particle size distribution that will affect the penetration characteristics and this is not accounted for by the current model.

For the case of the snow, the data were gathered with an helicopter hovering over a fresh snow field to create a whiteout. Independent measurements of the snow generation rate were not available. For the model, a snowfall rate of 230mm/hr was used, which would correspond to an extremely heavy snowfall observed by weather services. It can be noted that there is a significant discrepancy between the model and the measurements, due to the fact that a true whiteout model is unavailable.

Finally a measured detection range of ½" wires in clear conditions is shown with a close agreement with the model.

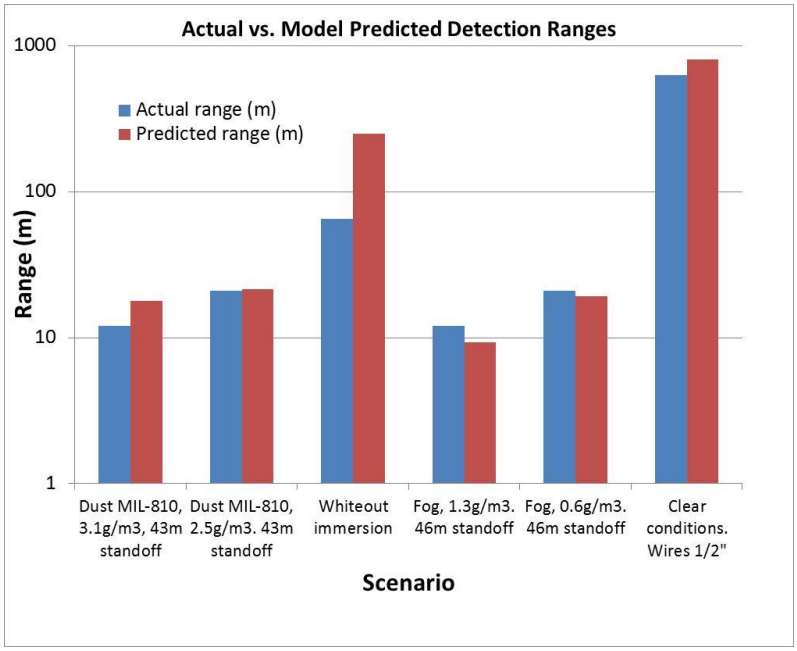

Figure 9. Comparison chart of measured versus predicted penetration ranges for few scenarios.

4. SENSOR EVOLUTION

For several applications, a full 360º azimuthal coverage or a very large field-of-view is ultimately desired. Neptec has developed a 360º full panoramic LiDAR, the OPAL-360, which is equipped with the same DVE penetration capability as the OPAL LiDAR prototype[8]. It was originally developed to address unique requirements of the Canadian Space Agency for a compact LiDAR that could simultaneously provide long-range terrain mapping, short range high-resolution feature examination, and autonomous navigation for a Mars Rover. Using a variant of the Risley prism pair approach, the sensor generates unique non-overlapping scan patterns that produce very dense 3D images with acquisition speeds of 200k points per second (PPS) at a range of 200m and 25k PPS up to a range of 3 km. The field of view can be up to 360ºx60º.

Figure 10 shows a picture on the left of the panoramic sensor OPAL-360. The picture on the right is a variant configuration where the unit uses a standard Risley prism pair to project rosette patterns in a circular field of view that can reach up to 120º. Not all applications require a panoramic scanner; however, applications such as aerial scanning will often require a large FOV. This family of LiDAR sensors is designed for harsh environments where poor visibility is often encountered.

Figure 10. OPAL sensor evolution into a full panoramic sensor (OPAL-360) and a large FOV projection (OPAL-120).

5. CONCLUSION

The paper summarized the obscurant penetration performances achieved by the OPAL obscurant penetration LiDAR. Examples included measurements done in dust, fog, snow and smoke. Where possible, the measurements were compared with predicted obscurants penetration performances based on the LiDAR equation for aerosols. An important lesson learned by the authors is the importance of conducting many well controlled experiments in order to understand the capabilities and limitations of a given instrument due to the complexity of the problem. Finally, the evolution of the OPAL sensor was presented as a viable option for harsh environments applications.

6. ACKNOWLEDGMENTS

The authors would like to thank Dr. Gilles Roy and Dr. Simon Roy from DRDC Valcartier. Part of this work was supported by DRDC Valcartier under contract W7701-10-3768 awarded to Neptec by Public Works and Government Services Canada.

7. REFERENCES

[1] Wadcock A., et al., "Rotorcraft downwash flow field study to understand the aerodynamics of helicopter brownout", AHS Southwest Region Technical Specialists' Meeting, Dallas, TX, Oct (2008).

[2] Roy, S., Cao X., Roy, G., Trickey E., "Evaluation of an obscurant-penetrating 3D-imaging LiDAR in whiteout conditions", 26th International Laser Radar Conference (ILRC), Porto Heli, Greece, June (2012).

[3] Seidel, C., Schwartz I., Kielhorn P., "Helicopter collision avoidance and brown-out recovery with HELLAS", Proc of SPIE 7114, 71140G-1, (2008)

[4] Savage J., Harrington W., McKinley R.A., Burns H.N., Braddom S., Szoboszlay Z., "3D-LZ helicopter ladar imaging system", Proc. of SPIE, 7684, 768407, (2010)

[5] Zhu X., Church P., Labrie M., "LiDAR for obstacle detection during helicopter landing", Proc of SPIE, 6950, 69500T-1, (2008).

[6] Short B., "3D Flash LADAR helicopter landing sensor for brownout and reduced visual cue", NAVAIR Public Release 11-033.

[7] Jelalian, A., [Laser Radar Systems], Artech House, Boston, (1992).

[8] Church P., Sekerka M., Trickey E., "Panoramic 360 Degrees Scanning LiDAR for Mobile Mapping and Survey", Proceedings of the International Lidar Mapping Forum, Denver CO, February (2013)